PHYSICAL REVIEW A VOLUME 14, NUMBER 4 OCTOBER 1976

Quantitative tunneling spectroscopy study of molecular structural changes due to electron irradiation

Mihir Parikh
IBM Thomas J. Watson Research Center, Yorktown Heights, New York 10598

James T. Hall and Paul K. Hansma
Department of Physics, University of California, Santa Barbara, California 93106
(Received 12 April 1976)

We have developed a new technique (utilizing inelastic electron tunneling spectroscopy) for the study of changes in molecular structure due to 30-keV electron irradiation. Analysis and interpretation of our experiments is done through the following: (1) an algorithm for fitting observed spectra with a series of fundamental peaks and thereby quantitatively provides the actual intensity of each peak; (2) a theory that determines the total (primary and secondary) electron fluence in the vicinity of the molecules and through the use of theoretical dissociation cross sections provides estimates of effective dissociation cross sections. Thus contributions of various molecular and geometrical properties to the degradation process can be delineated. Experimental data for β-*D*-fructose reveals that CH, CH_2 bonds are less susceptible to molecular degradation than the bonds in the COH functional group; also double bonds are formed. The strength and limitation of this technique are discussed.

I. INTRODUCTION

The deleterious effect of fast electrons on condensed molecular films is of great interest in radiation physics and chemistry; in particular, the atomic resolution of biomolecules in electron microscopy has not yet been achieved because of the destructive effect of the incident electrons. In order to minimize this effect, possibly via "tailoring" of molecules or by devising specimen geometries, it is necessary to develop a fundamental understanding of the degradation process and its dependence on molecular and geometrical parameters. Studies of changes in the molecular electronic structure,[1(a)] of changes in molecular crystallinity,[1(b)] and of changes in mass,[1(c)] yield information about the electron exposures necessary for particular changes to occur but cannot inherently yield information about changes in molecular bonding or structure. However, conventional (i.e., non-*in situ*) infrared spectroscopy of irradiated (bulk) films of polymers[1(d)] and nucleic acid bases[1(e)] does provide information about changes in molecular bonding and structure. Inelastic electron tunneling spectra/spectroscopy (IETS) shows great promise in explicitly providing *in situ* changes in bonding and structure of monolayers of adsorbed molecules.

IETS reveals[2(a)] the vibrational modes of organic compounds included in the insulating layer of a metal-insulator-metal tunneling junction. The effect of sandwiching the molecules between the metal electrodes apparently does not deform the physical structure of the molecules, since the vibrational frequencies from IETS correspond quite well to those from infrared and Raman spectra. Typically, a spectrum with a resolution of 16 cm^{-1} at a junction temperature of 4.2 K over a spectral range of 300–4000 cm^{-1} can be obtained.

This study presents preliminary data and analysis that reveals the strengths and weaknesses of IETS as a tool for radiation physicists. The experiments we describe below are of the simplest possible type; electron irradiation[3(a)] of the molecular film is done in the presence (or through) the metallic overlayer (Fig. 1). The overlayer serves as a screen against nucleating organic contaminants in the vacuum (10^{-5}–10^{-6} Torr) of our commercial scanning electron microscope. More sophisticated experiments could involve irradiation in the absence of the overlayer; this would, however, require sample preparation and irradiation in the same ultra-high-vacuum system. Interpretation of our experiments, involving irradiation through the overlayer, suffers from the following two complications: (1) The electron energy distribution and fluence[3(b)] in the vicinity of the molecular film is quite different from that in the primary beam. This can, however, be accounted for quite easily (Sec. III). (2) The overlayer leads to trapping of otherwise volatile fragments, thus possibly leading to the initiation of chemical reactions among fragments and metallic atoms. It is difficult to assess the magnitude of this effect from our experiments; however, more sophisticated *in situ* experiments should provide answers.

In order to analyze and interpret our experimental data, we have developed the following: (1) An algorithm and a computer program that fit a series of fundamental peaks to each spectrum (Sec. II A).

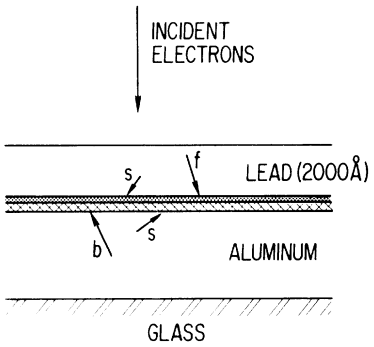

FIG. 1. Schematic diagram illustrating the geometry of the Al-Al_2O_3-organic-Pb junction on a glass substrate. The incident electrons generate forward-scattered (f), backscattered (b), and secondary (s) electrons, as shown schematically.

Thus true contributions from individual peaks are obtained for quantitative analysis. (2) A simple theory that determines the total [primary forward- and backward-scattered, as well as secondaries from both metals (see Fig. 1)] electron fluence in the vicinity of the molecules (Sec. III A) and through the use of theoretical dissociation cross sections provides estimates of effective degradation cross sections (Sec. III B). This theory seems particularly useful in elucidating the contributions from various molecular and geometrical properties.

II. EXPERIMENTS AND DATA ANALYSIS

IETS study of molecular structural changes induced by energetic electrons was done in three parts: (1) junction fabrication, (2) electron irradiation, and (3) spectrum measurement. Crossed film tunnel junctions, containing the molecules under study, were fabricated as follows[2(b)]: Al strips (0.1–0.2 mm wide, 2000 Å thick) were evaporated onto a glass slide in a clean, oil-free, high-vacuum evaporator. After removal from the vacuum system, the Al strips were allowed to oxidize in dust-free air briefly. The oxidized strips were then uniformly doped by spinning on a freshly made solution of β-*D*-fructose in water (0.5 mg/ml). Next the slide was returned to a high-vacuum evaporator, where four Pb strips (0.1–0.2 mm wide, 2000 Å thick) were evaporated across the doped, oxidized Al strips. Thus we obtain groups of four or five closely spaced (0.2—1.0 mm apart) junctions, on the same Al strip, with nearly the same characteristics.

Electron irradiation of the junctions (and thus the sandwiched molecules) were carried out in a scanning electron microscope (ETEC Autoscan). The junctions were electrically grounded by means of mechanical contacts between the strips and the sample holder. A slightly defocused beam was scanned over an area slightly larger than the junction area, thereby ensuring an even exposure of the entire junction. The irradiated area was determined by separately scanning a 200-mesh copper grid; the beam current was determined by scanning the beam within a Faraday cup. In most cases, all of the junctions on each substrate were given different electron fluences, except one which was left unexposed. Typical irradiation parameters were as follows: electron beam voltage, 30 keV; beam current, 0.2–60 nA; exposure time, 2–10 min (with a scan rate of 1 scan/sec); and pressure 10^{-5}–10^{-6} Torr.

After irradiation, the junctions were removed from the microscope and immersed in liquid He. The tunneling spectra [obtained as d^2V/dI^2 vs V] were measured using a second-harmonic detection technique that employed a 2-mV ac modulation at 1120 Hz and a second-harmonic voltage detection with a lock-in amplifier. Some results from our experiments with β-*D*-fructose are shown in Fig. 2. Two other experiments were performed to determine if the observed changes in the spectra were (1) dependent on the fluence rate or (2) due to heating of the junction by the electron beam. Figure 3 shows that the spectra depend on the total

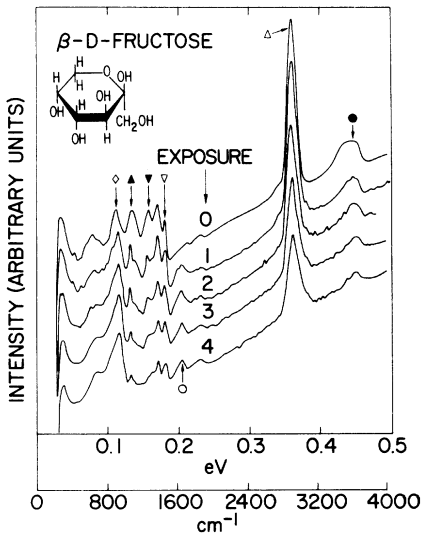

FIG. 2. IETS spectra of junctions containing β-*D*-fructose irradiated by 30-keV electrons for different incident electron exposures in a scanning electron microscope. Curves are labeled by a unit of exposure E_0 ~ 14 mC/cm^2. Each curve was traced in approximately 100 min with a lock-in sensitivity of 2 μV (full scale) and a time constant of 3 sec. Wave numbers: ▲, 1100; ▼, 1260; ▽, 1460; △, 2900; and ●, 3580 cm^{-1}. See text for further description.

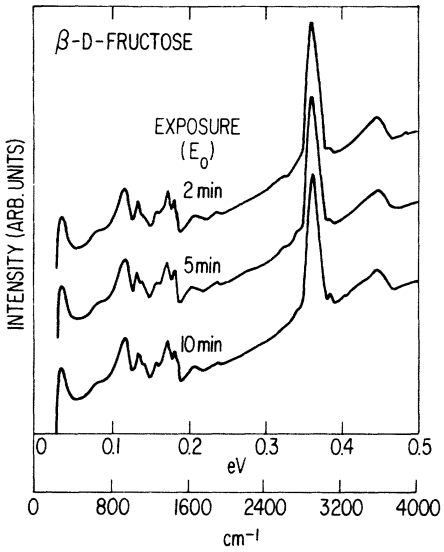

FIG. 3. Spectra showing exposure-rate independence of the degradation of β-*D*-fructose by 30-keV electrons.

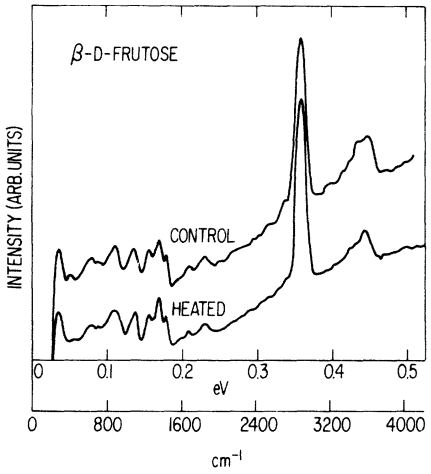

FIG. 4. Spectra showing no degradation in β-*D*-fructose by heating the junction to 110 °C for 45 sec; the control junction stayed below 70 °C.

electron fluence and not on the fluence rate; thus varying the electron beam current i and the exposure duration τ while keeping the total electron fluence ($\phi = i\tau$) constant produces the same spectrum. Figure 4 shows the results of a heating experiment. Samples identical to those used in the irradiation experiments were heated by holding a 60-W 400 °C soldering iron close to one end of a series of junctions. At the other end a heat sink was applied, so that a gradient of temperatures was obtained across the Al strip. The temperatures of the junctions were measured with temperature-sensitive paint applied directly over the junction area; in this way temperatures as high as 150 °C were maintained for ~1 min. While some junctions increased in resistance (and became electrically noisy) and others had melted lead strips, we never obtained degradation similar to that observed in the irradiation experiments. Simple calculations lead to estimates of maximum temperature rise of less than 50 °C under our experimental conditions.

The structure of β-*D*-fructose and the assignments of its vibrational bands are shown in Table I. The exact identification of the modes displayed by the IETS of fructose is somewhat questionable without isotopic shift studies and a better understanding of the exact species comprising the fructose molecular film in the tunneling junction. We have been using the nomenclature β-*D*-fructose without regard to possible changes of the morphology of this molecule adsorbed on the alumina substrate. *D*(-)levulose shows the same spectrum as β-*D*-fructose. Fructose is known to exist in three forms: (1) keto-*D*-fructose (chain configuration with carbon-oxygen double bond), (2) β-*D*-fructopyranose (six-member ring with a cyclic C–O–C group), and (3) β-*D*-fructofuranose (five-

TABLE I. Structure and vibrational assignments of β-*D*-fructose.

Assigned modes	Symbol in Fig. 2	Reference number	Bands in tunneling spectra (cm^{-1})	Bands in ir spectra (cm^{-1})
ν(OH)	●	4	3580	3450, 3550
$\nu(CH, CH_2)$	△	5	2920	2860, 2940
$\nu(CH_2$ scissor)	▽	5	1460	1460
$\beta(OH)/\beta(CH_2)$?		6	1380	1370, 1400
β(OH)	▼	4	1260	1265
ν(CO), ν(C–O–C)	▲	4	1070, 1145	1080, 1150
Symmetric ring structure		7	930	923, 928
Ring mode		7	850, 870	822, 872
Ring breathing		7	780?	784

member ring with a cyclic C–O–C group).[7(a)] The true geometry of our molecular film of fructose is complicated by chemical or physical adsorption changes that could occur upon doping the alumina substrate. (For instance, benzaldehyde, upon doping on alumina, becomes a benzoate ion, losing the carbon-oxygen double bond.[2(c)]) Since our IETS of fructose shows no CO double-bond stretching mode and no asymmetric carboxylate stretching mode, we assume our fructose to be in a ring conformation.

The COH functional groups in the fructose molecule can be expected to have three strong vibrational bands at positions close to those found[4] for this functional group in primary and tertiary alcohols. These are a CO stretching vibration in the range 1050–1150 cm^{-1}, an OH bending vibration in the range 1260–1300 cm^{-1}, and an OH stretching vibration around 3600 cm^{-1}. Figure 2 shows that there are three strong bands at these wave numbers. The mode at 1100 cm^{-1} is actually comprised of two modes, one at 1070 and another at 1145 cm^{-1}, probably corresponding to ν(C–O–C) and ν(C–OH). The large broad peak at 2900 cm^{-1} can be unambiguously associated[5] with CH and CH_2 vibrational modes. The peak at 1460 cm^{-1} can be associated[5] with the scissorlike vibration of CH_2. The peak at 1380 cm^{-1} can probably be assigned[4,6] to an OH and/or CH bending modes); however, this is uncertain at present. Infrared study[7(b)] of 2-keto sugars has made it possible to assign a mode at 925 cm^{-1} to a ring stretching vibration; other modes dependent on molecular configuration are observed at 872, 822, and 781 cm^{-1}. In this region a tunneling spectrum of a junction with an Al_2O_3 insulator has[2] a prominent broad mode at 920 cm^{-1}. Even though the exact location of the ring modes are masked by this broad peak, one can associate the shoulder at 880 cm^{-1} with a ring mode.

A. Data analysis

The quantitative analysis of changes in the IETS due to changes in the molecular structure must involve the determination of the true contribution of each band. This can be done through a nonlinear least-squares fit of the data with a function consisting of a series of fundamental peak shapes and a background. The background contribution is due primarily to elastic tunneling; the elastic tunneling current I_e can be approximated[8] for small values of V by

$$I_e = \alpha(V + \gamma V^3). \tag{1}$$

Thus the inelastic tunneling characteristic d^2I_{in}/dV^2, which is the difference between the measured (total) tunneling characteristic d^2I/dV^2 and the elastic tunneling characteristic d^2I_e/dV^2, can be written

$$\frac{d^2I_{in}}{dV^2} = \frac{d^2I}{dV^2} - 6\alpha\gamma V. \tag{2}$$

Theoretically a peak in the inelastic tunneling characteristic d^2I_{in}/dV^2 can be written[9] as a convolution product of three functions:

$$\frac{d^2I_{in}}{dV^2} = n_0(\hbar\omega_0)[D^*\chi^*\phi]. \tag{3}$$

The number of molecules participating in a particular vibrational mode ($\hbar\omega_0$) is $n_0(\hbar\omega_0)$; $D(\hbar\omega_0)$ is the spectral weight function[10,2(a)] of that vibrational mode; ϕ is the instrumental modulation function[9] given by

$$\phi(E) = \begin{cases} \frac{8}{3\pi}\frac{1}{(eV_\omega)^4}[(eV_\omega)^2 - E^2]^{3/2}, & \text{for } |E| < eV_\omega, \\ 0, & \text{for } |E| \geq eV_\omega, \end{cases} \tag{4}$$

where V_ω is the modulation voltage applied to the junction in a second-harmonic measurement of IETS; χ is the thermal function[2(a)] given by

$$\chi(x) = \frac{1}{kT}\frac{e^x[(x-2)e^x + x + 2]}{(e^x - 1)^3}, \tag{5}$$

where $x = |E - eV|$ and V is the bias voltage across the junction. In principle, the shape of a fundamental peak can be obtained by performing the convolutions in Eq. (3); however, the form of the spectral weight function $D(\hbar\omega_0)$ is not known. Figure 5 shows the result obtained on convoluting the thermal and instrumental functions [Eqs. (4) and (5)] for typical values of eV_ω/kT. A nonlinear least-squares program has been used to fit the peaks shown in Fig. 5 with a Lorentzian or a Gaussian with adjustable widths and heights. While neither the Lorentzians nor the Gaussians provide a perfect fit to these peaks, the Gaussians do show a much better fit to the "tail" of the function. Thus the Gaussian approximation for the peak shapes is expected to yield smaller errors in the fitting of several overlapping peaks, as in the case of IETS.

A computer program has been developed to simultaneously fit a series of Gaussians to the IETS. The purpose of such a fit is to be able to determine the area and position of individual peaks in IETS. The following algorithm has been used to fit all of the data:

(1) The background due to elastic tunneling is determined by fitting a straight line to the data between 1800 and 2600 cm^{-1}. The slope of the background (which varies less than 10% between junctions) is used to normalize intensity of individual peaks; this makes comparison of peak

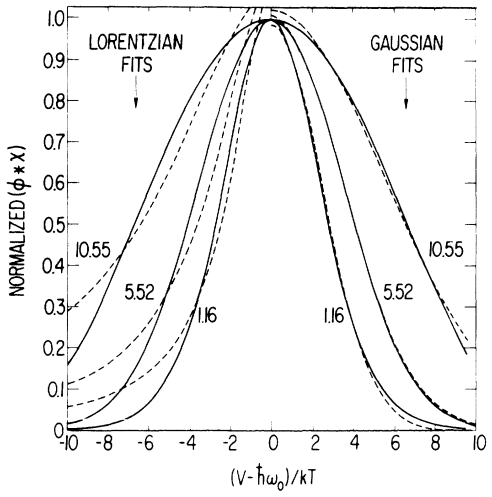

FIG. 5. Fit of Gaussians and Lorentzians (dashed curves) to numerically calculated peak shapes obtained by convolving the instrumental and thermal functions. Values of eV_ω/kT correspond to combinations of $T = 10$, 4.2, and 1.1 K, and $eV_\omega = 1.0$ and 2.0 meV.

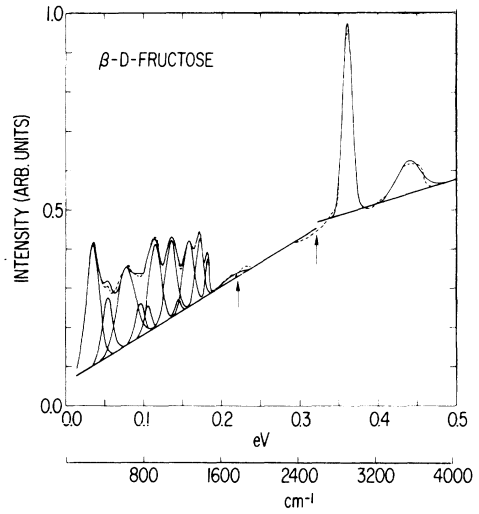

FIG. 6. Nonlinear least-squares fit of spectrum (dashed curve) of undamaged β-D-fructose to a series of Gaussians (solid curves) with adjustable parameters. The background is determined by a linear least-squares fit of data in the region included by the two arrows.

intensities between junctions quantitative.

(2) As indicated in Eq. (2), the background is subtracted from the data to yield the purely inelastic characteristic d^2I_{in}/dV^2.

(3) For the data between 300 and 1900 cm^{-1}, 12 fundamental peaks (nine indicated in Table I and peaks at 280, 650, and 1800 cm^{-1}) are used as initial guesses in the fitting program. The program determines peak positions, areas, and widths (full width at half-maximum) in the least-squares sense. Typical fits with variances of 0.02 are obtained, requiring a computing time of 0.3 min on the IBM 370/168.

(4) For the data between 2700 and 4000 cm^{-1}, only two peaks, at 2920 and 3580 cm^{-1}, are used as initial guesses.

Along with the elastic tunneling background, the spectrum of the "clean" (undoped) junction has to be considered. Formal subtraction of the "clean" junction spectrum for our spectra of β-D-fructose is not possible at present; thus we cannot quantify the intensities of the following: (1) The 3580 cm^{-1} peak, which contains contributions from ν(OH) in fructose as well as the aluminum hydrate stretch in the oxide; (2) the peaks below 1000 cm^{-1}, in particular the aluminum hydrate OH bending mode at 920 cm^{-1}; since various ring modes of fructose lie in this region, we cannot at present quantify these peaks without formal "subtraction" of the 920-cm^{-1} peak.

A typical fit is shown in Fig. 6; the behavior of the intensities (or areas) of individual peaks as a function of incident electron exposure is shown in Fig. 7. Notice that the modes belonging to the CH, and CH_2 bonds decrease at a considerably slower rate with respect to incident electron exposure than the modes belonging to the COH functional group. Also, while the CH and CH_2 modes have an approximately exponential dependence on E (especially the mode at 3580 cm^{-1}), the COH modes have a distinctly nonexponential dependence. A possible explanation for this is discussed in Sec. III B. Finally, note that while no modes existed at ~1600 cm^{-1} in the nonirradiated β-D-

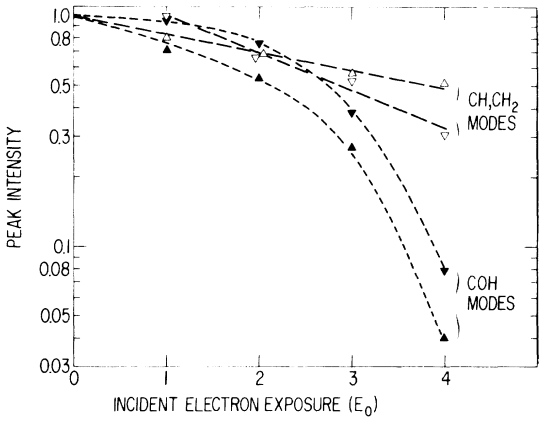

FIG. 7. Peak intensity (denoted by symbols) variation of various modes in β-D-fructose as a function of incident electron exposure (in units of E_0). Dashed curves merely illustrate trend and are not fits to data. Data points have an accumulated error of ~ 10–15%, due to errors in spectrum measurement and fitting.

fructose spectrum (Fig. 2), a strong mode develops (and persists) with increasing irradiation. This mode is attributable[5] to $\nu(C=C)$ and possibly to $\nu(C=O)$. Thus one can conclude at present that the effect of irradiation is to disrupt bonds in the CH, CH_2, and COH functional groups while forming C = C and possibly C = O bonds.

III. MOLECULAR DEGRADATION AND ELECTRON EXPOSURE

In this section we develop a relationship between the number of damaged molecules and the incident electron exposure. The aim of this analysis is as follows: (1) To delineate the effect of the overlayer and of the substrate on the measured degradation, in particular, the effect of the primary and secondary electrons on the sandwiched molecules, and (2) to attempt to answer questions such as: Is it possible to deduce degradation cross sections of molecules from the measured spectra? Conversely, can the changes in spectra (or molecular structure) be predicted if the free molecule's dissociation cross sections are known? To achieve this aim, the total electron fluence in the neighborhood of the sandwiched molecules is determined and is then convolved with molecular dissociation cross sections. This formulation can be directly related to intensity changes in the IETS, because the number of molecules participating in a particular molecular vibration is proportioned to the intensity of the corresponding band in the IETS.

The decrease in the number of undamaged molecules, n, due to incident electron exposure dE is given by

$$dn = -n\sum_i\sum_j df_j^i, \tag{6}$$

where df_j^i is the fraction of molecules damaged via several possible processes (j) that were initiated by primary or secondary electron fluences (i). The fractional damage df_j^i can be written in terms of $\sigma_j(T)$, the cross section for molecular dissociation occurring via process j, and in terms of $D_i(T, T_0)\,dE$, the distribution of electron fluence of type i

$$df_j^i = \int \sigma_j(T) D_i(T, T_0)\,dE\,dT. \tag{7}$$

Here dE is the incident exposure [in electrons/(unit area)] of electrons of energy T_0 and $D_i(T, T_0)$ is the energy distribution of electrons in the vicinity of the molecules (i.e., at the interface of lead and aluminum).

A. Electron fluence

The electron fluence at the molecular film is due to both primary (forward- and backward-scattered) electrons as well as secondary electrons (Fig. 1).

The energy *distribution of primary electrons* at the molecular film $D_p(T, T_0)$ has been calculated by a Monte Carlo simulation[11] of electron trajectories. The Monte Carlo model used[12] is particularly suitable for our calculations, since it explicitly considers energy loss as a probabilistic process[13] rather than through the "continuous-slowing-down" approximation. The sandwiched structure is modeled simply as a film of amorphous lead on an infinitely thick amorphous aluminum substrate. The calculations were performed with at least 10 000 incident electrons, so that a statistical accuracy of better than 1% is obtained. For the case of a 2000-Å lead film on aluminum (which corresponds to experimental arrangement), Fig. 8 shows the calculated primary electron distribution $D_p(T, T_0)$, as well as the contributions from the forward- and backward-scattered primary electrons. Note that we have plotted the dimensionless quantity $m\delta T_0 D_p(T, T_0)$; this is merely the number of electrons traversing the interface with energy in the interval $(T + \frac{1}{2}\delta T_0,\ T - \frac{1}{2}\delta T_0)$. Also, we calculate the quantities Δ_0 and Δ_{12}, which are, respectively, the average number of crossings of the interface by a primary electron and the probability of an electron between T_1 and T_2 crossing the interface. As Fig. 8 indicates, for every ten (incident) electrons, on the average 13 electrons cross the interface. Of these ~nine travel in the forward direction (with 0.73 probability of energy between

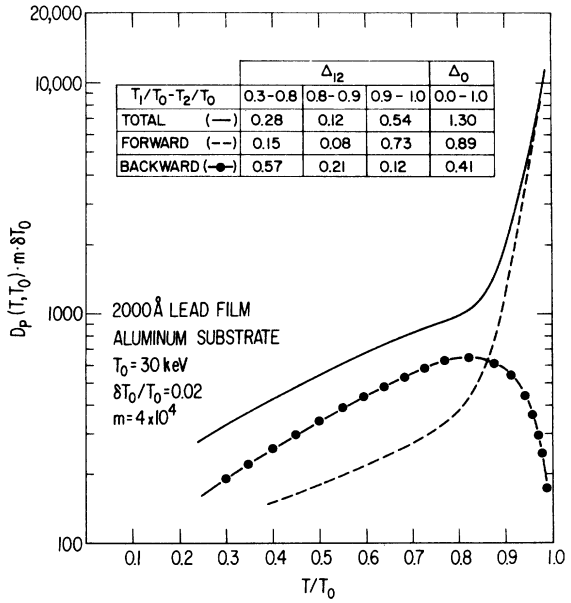

	Δ_{12}			Δ_0
T_1/T_0-T_2/T_0	0.3-0.8	0.8-0.9	0.9-1.0	0.0-1.0
TOTAL (—)	0.28	0.12	0.54	1.30
FORWARD (--)	0.15	0.08	0.73	0.89
BACKWARD (-●-)	0.57	0.21	0.12	0.41

FIG. 8. Energy distribution of total (solid), forward- (dashed), and backward- (dotted) scattered electrons at the interface of a 2000-Å lead film and aluminum substrate due to 30-keV incident electrons.

$0.9T_0$ and T_0), while four electrons are scattered backwards from the aluminum substrate (with 0.57 probability of having energy between $0.3T_0$ and $0.8T_0$). The skewness of this distribution will lead to major simplifications in the calculation of Eq. (6).

The *distribution of secondary electrons* is obtained by convolving the primary electron distribution at the interface $D_p(T, T_0)$ with a secondary electron distribution function dN_s/dT. The use of $D_p(T, T_0)$ is justified on consideration that all secondary electrons that appear at the interface were generated within a distance $\lesssim 200$ Å from the interface. Thus

$$D_s(T, T_0) = \int_0^\infty \frac{dN_s}{dT}(T, T') D_p(T', T_0)\, dT'. \tag{8}$$

The secondary electron distribution dN_s/dT is obtained from a simple theory[14] and recent experimental data.[15] We obtain

$$\frac{dN_s}{dT}(T, T') = 6\delta_0(T')\Phi^2 \frac{T}{(T+\Phi)^4}, \tag{9}$$

where $\delta_0(T')$ is the secondary electron coefficient for the emission of secondary electrons initiated by an incident electron of energy T' from a material with work function Φ; Fig. 9 shows a typical dN_s/dT. The approximations and assumptions involved in the derivation of Eq. (9) are discussed elsewhere[12]; here it suffices to note that this simple expression provides a maximum at $T = \frac{1}{3}\Phi$ and agrees well with experimental data.[14] Since secondary electrons are generated by both aluminum and lead, Eq. (8) contains an implicit summation over the two metals.

B. Molecular degradation

The influence of the primary and secondary electrons on the molecules can now be discussed by considering the various processes for molecular dissociation. The significant processes are dissociative ionization (DI) and dissociative attachment (DA):

$$\begin{aligned} &AB + e^- \rightarrow A^+ + B + 2e^- \quad \text{(DI)}, \\ &AB + e^- \rightarrow A^- + B \quad \text{(DA)}. \end{aligned} \tag{10}$$

Here A and B are fragments of a molecule AB. The "knock-on" process (i.e., atomic displacement of atomic nuclei via direct momentum transfer) is ignored, since it has[16] a very small cross section ($< 10^{-20}$ cm^2) for incident electron energies ~ 30 keV.

While the magnitude of the cross sections for each of the processes in Eq. (10) for a given molecule may be unknown, the general form of the cross sections are known. For DI, the threshold behavior is[17] not too different from the 1.0–1.127 power law[18] for ionization thresholds. Thus we write

$$\sigma_{DI}(T) \sim \alpha_{DI}(T - \tau_{DI})^\beta, \quad \text{for } T > \tau_{DI}, \tag{11}$$

where τ_{DI} is the threshold energy for DI and β is a parameter of the model. For simplicity, we assume (Fig. 9) a linear threshold ($\beta = 1$) behavior of σ_{DI}. The behavior of σ_{DI} for large incident electron energies is similar[17,19] to the behavior of ionization cross sections[20]; i.e.,

$$\sigma_{DI}(T) = (k/T)\ln(T/B), \tag{12}$$

where

$$k = \sigma_{DI}(T_0)\frac{T_0}{\ln(T_0/B)},$$

and B is a parameter that depends on the properties of the molecule. The DA cross sections are well known[21] to have the form

$$\sigma_{DA}(T) = \frac{C_{DA}}{T/\tau_{DA}} \exp\left(-\frac{(T-\tau_{DA})^2}{(\Gamma_{DA})^2}\right) e^{-\rho(T)}, \tag{13}$$

where $\tau_{DA} - \frac{1}{2}\hbar\omega$ is the electron energy at the peak of σ_{DA}, $\frac{1}{2}\hbar\omega$ is the zero-point energy, Γ_{DA} is the experimentally determined full width, and $\rho(T)$ is the survival probability of the negative molecular ion.

The fractional damage induced by primary and secondary electrons by the processes of DI and DA can now be estimated. The estimation is particularly simplified by the highly skewed distribution $D_p(T, T_0)$ of electrons at the interface. For DI induced by primary electrons, Eqs. (7) and (12) yield

$$df_{DI}^p = \kappa\, \sigma_{DI}(T_0)\Delta_0\, dE, \tag{14}$$

where κ depends very weakly on B (Fig. 10). Thus df_{DI}^p can be estimated without concern for the exact form of σ_{DI}, but with the knowledge of only

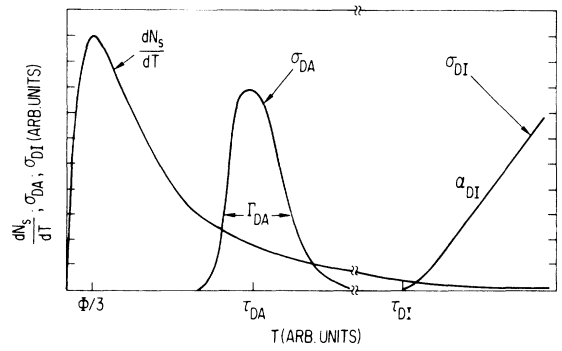

FIG. 9. Schematic diagram illustrating typical behavior of secondary electron energy distribution dN_s/dT, and dissociative ionization and attachment cross sections (σ_{DI} and σ_{DA}) as a function of incident electron energy T.

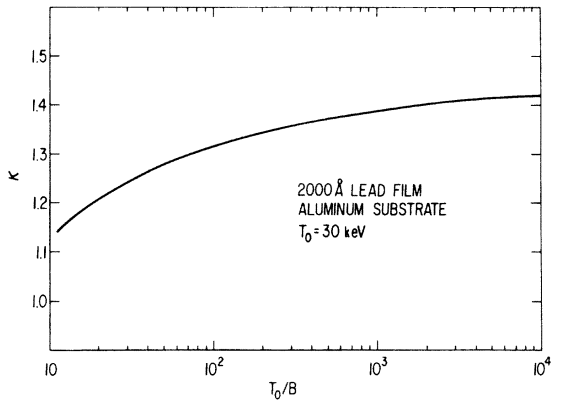

FIG. 10. Variation of parameter κ with T_0/B for electrons with $T_0 = 30$ keV.

$\sigma_{DI}(T_0)$ and Δ_0. For degradation induced by secondary electrons, Eq. (7)–(9) yield

$$df_j^s = \kappa' \Delta_0 \int \sigma_j(T) \frac{dN_s}{dT}(T, T_0)\, dT\, dE, \tag{15}$$

where $\delta_0(T')$ has been assumed[12,22] to have a $(1/T')\ln T'$ dependence. As before, κ' depends on B (Fig. 10). Evaluation of the integral over T in (15) requires the knowledge of $\sigma_j(T)$ for $T \lesssim 100$ eV. In the case of DI induced by slow electrons, Eq. (15) and (11) yield

$$df_{DI}^s = \kappa' \delta_0(T_0) \Delta_0 \alpha_{DI} g_{DI}^s(\tau_{DI}, \Phi)\, dE, \tag{16}$$

where

$$g_{DI}^s(\tau_{DI}, \Phi) = \Phi^2(3\tau_{DI}^2 + \tau_{DI}\Phi + 2\Phi^2)/(\tau_{DI} + \Phi)^3.$$

In the case of DA induced by slow electrons, Eqs. (15) and (13) yield

$$df_{DA}^s = \kappa' \delta_0(T_0) \Delta_0 C_{DA} g_{DA}^s(\tau_{DA}, \Gamma_{DA}, \Phi)\, dE, \tag{17}$$

where g_{DA} is obtained via a numerical integration; Fig. 11 shows the behavior of g_{DA}^s as a function of Γ_{DA} and τ_{DA}.

It is now possible to make estimates regarding the contributions of the various processes to the degradation of molecules included between the 2000-Å lead film and the aluminum substrate. Combining Eqs. (14), (16), and (17) we can write

$$-dn/n = \kappa \Delta_0 \{\sigma_{DI}(T_0) + \alpha_{DI}[(\delta_0 g_{DI}^s)_{Al} + (\delta_0 g_{DI}^s)_{Pb}] + C_{DA}[(\delta_0 g_{DA}^s)_{Al} + (\delta_0 g_{DA}^s)_{Pb}]\}\, dE. \tag{18}$$

The first term on the right-hand side is due explicitly to the action of primary electrons, where DI is considered to be the primary process. The other two sets of terms are due to DI and DA, respectively, with individual contributions from Al and Pb explicitly indicated. Note that since κ depends weakly on B, we have assumed for simplicity in Eq. (18) that $\kappa \sim \kappa'$.

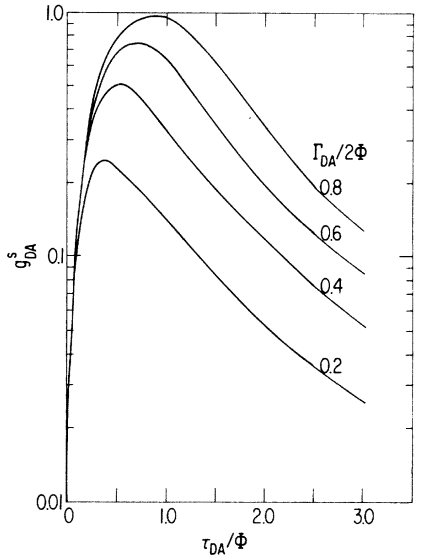

FIG. 11. Behavior of the parameter g_{DA}^s as a function of τ_{DA}/Φ.

Integration of Eq. (18) yields a purely exponential dependence for the survival of molecules as a function of incident electron exposure. Thus

$$n(E) = n_0 e^{-\sigma_D E}, \tag{19}$$

where n_0 is the initial concentration of undamaged molecules (exhibiting the vibrational mode under consideration) and σ_D is the net degradation cross section given by the product of $\kappa\Delta_0$ and the term in curly brackets on the right-hand side of Eq. (18). In general the formalism of Eq. (18) has to be extended to include intermolecular interactions. Somewhat simplistically one can include the effects of dissociation and recombination (or healing) induced by intermolecular interactions and write

$$dn = -n\sigma_D dE - \lambda_d n^2 dE + \lambda_h n^2 dE, \tag{20}$$

where λ_d and λ_h are intermolecular coupling parameters that characterize dissociation and healing, respectively. Integration of (20) yields

$$\frac{n(E)}{n_0} = \left[\left(1 + \frac{\lambda n_0}{\sigma_D}\right) e^{\sigma_D E} - \frac{\lambda n_0}{\sigma_D}\right]^{-1}, \tag{21}$$

where $\lambda = \lambda_d - \lambda_h$ is the effective coupling constant. When intermolecular healing dominates intermolecular dissociation, λ is negative and a shoulder in the $\ln(n/n_0)$ vs E curves (survival curves) is obtained.

The above analysis allows us to make the follow-

ing observations about the degradation of β-*D*-fructose: (1) The approximately exponential dependence of the CH and CH_2 modes (Fig. 7) suggests that the degradation process for these modes involves little intermolecular coupling. The σ_D for the disruption of these bonds is ~0.02–0.03 Å^2. (2) The shoulders in the survival curves for the modes belonging to the COH functional group seem to imply that some intermolecular or interaction with the substrate/overlayer atoms has occurred. For these COH bonds, the σ_D is ~0.10–0.15 Å^2, while an effective intermolecular coupling constant is obtained from $\lambda n_0/\sigma_D$, which is ~0.95.

In order to assess the effect of the overlayer/substrate on the degradation of the sandwiched molecules, the magnitude of the DI and DA cross sections are needed; while for fructose these are unavailable, for two model molecules (CH_4 and C_6H_5Br) these are available.[17,23] Table II shows the calculated *effective* DI and DA cross sections. The effective DI cross section is greater than the effective DA cross section, in agreement with analogous free molecular cross sections. However, DI induced by fast (30 keV) electrons [given by the first term on the right-hand side of (18)] is also quite likely, since[17] $\sigma_{DI}(30\text{ keV}) \sim 0.1 \times \sigma_I(30\text{ keV}) \sim 6\times10^{-19}$ cm^2. Thus for a molecule like CH_4 both secondary and primary DI processes play important roles. In the case of a molecule like C_6H_5Br, large DA cross sections lead to large secondary-electron-initiated effective DA cross sections; in such molecules, degradation would occur almost exclusively via DA. These calculations lead to some generalizations: (1) The contribution of the Pb overlayer to the effective DI and DA cross sections is only ~1.5 times that of the Al substrate, in spite of the large difference in Z between Al and Pb. (2) The effective DI cross section is determined so strongly by the form of dN_s/dT that it seems to be essentially independent of the molecular species and is generally of the order of 10^{-20} cm^2. (3) The effective DA cross section is generally about 60–100 times smaller than the maximum of the free molecular DA cross section; this is partly due to the magnitude of δ_0 being of the order of ~0.1. Finally, note that while our formulation (Eq. 7) required the knowledge of molecular *dissociation* cross sections, we also need the probability that a molecule will remain fragmented after dissociation. Depending on the environment, fragments can either react with other fragments or metal atoms from the substrate/overlayer or they can recombine. Probabilities for these processes are unknown. Only detailed experiments involving irradiation of the molecules both through a thin overlayer and in the absence of an overlayer can answer some of the questions about magnitude of fragment trapping/reacting with the overlayer.

TABLE II. Effective DI and DA cross sections [a] (in units of cm^2).

		Al $\delta_0=0.087$ $\Phi=4.18$ eV	Pb $\delta_0=0.130$ $\Phi=3.83$ eV
CH_4 [b]	σ_{DI}^{eff}	1.0×10^{-20}	1.5×10^{-20}
	σ_{DA}^{eff}	1.1×10^{-21}	1.6×10^{-21}
C_6H_5Br [c]	σ_{DI}^{eff}	3.0×10^{-20}	4.2×10^{-20}
	σ_{DA}^{eff}	1.6×10^{-18}	2.8×10^{-18}

[a] $\sigma_{DI}^{eff} \equiv \alpha_{DI}(\delta_0 g_{DI}^s)_i$, $\sigma_{DA}^{eff} \equiv c_{DA}(\delta_0 G_{DA}^s)_i$; i stands for Al or Pb.

[b] Parameters for CH_4: $\alpha_{DI} \sim 3.5\times10^{-19}$ cm^2/eV; $\tau_{DI} \sim 25$ eV; $c_{DA}=9.0\times10^{-20}$ cm^2; $\tau_{DA}=10$ eV; $\Gamma_{DA} \sim 2.6$ eV.

[c] Parameters for C_6H_5Br: $\alpha_{DI} \sim 10^{-18}$ cm^2/eV; $\tau_{DI} \sim 25$ eV ("worst-case" estimates); $c_{DA}=9.5\times10^{-17}$ cm^2; $\tau_{DA}=0.85$ eV; $\Gamma_{DA} \sim 0.92$ eV.

IV. CONCLUSION

The simplest of all possible experiments involving the application of IETS to energetic electron induced molecular degradation has shown the following: (1) Some bonds are more resistant to degradation than others. New double bonds are formed. In particular, the degradation of fructose produces a decrease in saturated (CH, CH_2) bonds, creates new conjugated bonds (C=C and C=O), and disrupts bonds in the COH functional group more readily than other bonds. (2) Data can be quantified by means of a nonlinear least-squares fit to a series of fundamental peaks to ~90% accuracy. (3) The shape of the survival curves indicates that some intermolecular effects may be occurring.

Interpretation of the degradation is possible on consideration of the total (primary and secondary) electron fluences and typical degradation cross sections. In particular, the highly skewed energy distribution of electrons at the interface allows for major simplification in $D_p(T, T_0)$, i.e., $D_p(T, T_0) \rightarrow \Delta_0 \kappa \delta(T - T_0)$. (Here δ is the Dirac δ function.) Simple models for secondary electron fluence from the substrate and the overlayer (with parameters δ_0 and Φ) and for dissociation cross sections result in simple expressions for effective degradation cross sections. The utility of this analysis is that contributions to total degradation due to substrate/overlayer geometry and properties as well as molecular properties (via DI or DA cross sections) can be easily delineated. In summary, we believe that considering the encouraging results obtained from our preliminary analysis of our simple ex-

periments, more sophisticated (*in situ*) experiments and more detailed analysis is warranted.

ACKNOWLEDGMENTS

We thank T. E. Everhart and H. Hansma for discussions. One of us (M. P.) is thankful to his colleagues at IBM, in particular to T. Penny for the use of his data digitization facilities; to E. Munro and P. S. Wolfe for advice on the development of a nonlinear least-squares program; to R. Pollak for assistance in and use of a new fitting program, GAMET; and to D. F. Kyser for advice and a copy of a Monte Carlo program for electron scattering. Thanks also to M. S. Chung for discussions on secondary electron energy distribution.

[1](a) M. Isaacson, D. Johnson, and A. V. Crewe, Radiat. Res. 55, 205 (1973); (b) R. M. Glaeser, J. Ultrastruct. Res. 36, 466 (1971); (c) J. Wall, Ph.D. thesis (Univ. of Chicago, 1971) (unpublished); (d) G. Bahr., F. Johnson, and E. Zeitler, Lab. Invest. 14, 1115 (1965); (e) M. A. Marcus and J. Corelli, Radiat. Res. 57, 20 (1974).

[2](a) J. Lambe and R. C. Jaklevic, Phys. Rev. 165, 821 (1968); (b) P. K. Hansma and R. V. Coleman, Science 184, 1369 (1974); (c) M. G. Simonsen, R. V. Coleman, and P. K. Hansma, J. Chem. Phys. 61, 3784 (1974).

[3](a) P. K. Hansma and M. Parikh, Science 188, 1304 (1975); (b) Electron microscopists commonly use the term "electron exposure" or "electron dose" to denote incident charge per unit area. The standard term for such a quantity, recommended by the International Commission on Radiation Units and Measurements [in *Radiation Quantities and Units* (Report No. 19, International Commission on Radiation Units and Measurements, Washington, D. C., 1971)] is the electron "fluence"; henceforth we shall use this term.

[4]R. T. Conley, *Infrared Spectroscopy*, 2nd ed. (Allyn and Bacon, Boston, 1972).

[5]K. Nakanishi, *Infrared Absorption Spectroscopy* (Holden-Day, San Francisco, 1962).

[6]H. A. Szymanski, *Theory and Practice of Infrared Spectroscopy* (Plenum, New York, 1964).

[7](a) C. Barry and J. Honeyman, Adv. Carbon Chem. 7, 53 (1952); (b) L. M. J. Verstraeten, Anal. Chem. 36, 1040 (1964).

[8]J. M. Rowell, in *Tunneling Phenomena in Solids*, edited by E. Burstein and S. Lundqvist (Plenum, New York, 1969).

[9]J. Klein *et al.*, Phys. Rev. B 7, 2336 (1973).

[10]D. J. Scalapino and S. M. Marcus, Phys. Rev. Lett. 18, 459 (1967).

[11]K. Murata, T. Matsukawa, and R. Shimizu, Jpn. J. Appl. Phys. 10, 678 (1971).

[12]M. Parikh, J. Hall, and P. K. Hansma, IBM Report No. RC5953 (unpublished).

[13]R. Shimizu *et al.*, J. Phys. D 8, 820 (1975).

[14]M. S. Chung and T. E. Everhart, J. Appl. Phys. 45, 707 (1974).

[15]R. Shimizu, J. Appl. Phys. 45, 2107 (1974).

[16]M. Parikh, Ph.D. thesis (Univ. of California at Berkeley, 1974) (unpublished).

[17]D. Rapp, P. Englander-Golden, and D. D. Briglia, J. Chem. Phys. 42, 4081 (1965).

[18]M. R. H. Rudge, Rev. Mod. Phys. 40, 564 (1968).

[19]M. Parikh, Phys. Rev. A 12, 1872 (1975).

[20]M. Inokuti, Rev. Mod. Phys. 43, 297 (1971).

[21]J. N. Bardsley, A. Herzenberg, and F. Mandl, Proc. Phys. Soc. Lond. 89, 321 (1966); T. F. O'Malley, Phys. Rev. 150, 14 (1966).

[22]M. Parikh and R. Shimizu, Appl. Phys. Lett. (to be published).

[23]L. G. Christophorou, *Atomic and Molecular Radiation Physics* (Wiley, New York, 1970).